DOI: 10.47743/achi-2025-1-0004 *ACTA CHEMICA IASI*, **33_1**, 61–82 (2025)

PHOTOPHYSICS OF Y_2O_3:ZnPc(COOH)$_4$ ASSEMBLIES

Tamara Potlog[a], Ion Lungu[a*], Alexandrina Druta[b]

[a]*Laboratory of Organic/Inorganic Materials for Optoelectronics, Moldova State University, Alexei Mateevici St 60, Chişinău, Republic of Moldova*

[b]*Doctoral School "Natural Sciences", Moldova State University, Alexei Mateevici St 60, Chişinău, Republic of Moldova*

Abstract: Yttrium oxide nanoparticles were conjugated separately to zinc tetracarboxy phthalocyanine (ZnPc(COOH)$_4$) to form Y_2O_3:ZnPc(COOH)$_4$ assemblies. The triplet quantum yields and lifetimes of the phthalocyanines increased following conjugation. The resulting assemblies exhibited stronger fluorescence with increased quantum yields, reaching up to 33.44% compared to ZnPc(COOH)$_4$ alone, which has a value of 0.3%. The triplet quantum yields increased from Φ_T = 14.8% for ZnPc(COOH)$_4$ to Φ_T = 29.9% and 30.9% for the Y_2O_3:ZnPc(COOH)$_4$ assemblies. The lifetimes also became longer for the conjugates compared to ZnPc(COOH)$_4$ alone. These studies open new avenues for the development of next-generation phosphorescent materials with tailored functionalities for both industrial and medical applications.

Keywords: absorbance, fluorescence, phosphorescence, excited state lifetime, quantum yield.

Introduction

Yttrium oxide (Y_2O_3) nanoparticles (NPs) have excellent photoluminescence (PL) properties and have been used in various applications, such as diagnostics, imaging, optics, and the biomedical field.[1–4]

*Ion Lungu, *e-mail:* ionlungu.usm@gmail.com

Y_2O_3 NPs are renowned for their exceptional optical properties, including luminescence, which can be enhanced by doping with rare-earth ions such as erbium (Er^{3+}).[1] The europium-doped yttrium oxide ($Y_2O_3:Eu^{3+}$) phosphor is well known for producing intense red emission under UV short-wavelength (210 – 255 nm) excitation. However, this limits the use of $Y_2O_3:Eu^{3+}$ in converting near-UV photons (300 – 400 nm) to red photons ($\lambda \sim 612$ nm) for white LED applications.[5-7]

Metallophthalocyanine (MPc) complexes are widely used as photosensitizers in photodynamic therapy (PDT),[8-12] due to their low dark toxicity, strong absorption in the red region of the electromagnetic spectrum, high stability, and efficient singlet oxygen generation.[13,14] Substitution of the peripheral positions of ZnPc with carboxyl (COOH) groups improves solubility and biocompatibility, while promoting interactions with nanoparticles, which can improve energy transfer efficiency and photophysical properties.[3] Studies have shown that these structural modifications significantly affect the photophysical properties of ZnPc, especially its singlet oxygen generation capacity.[15] The combination of the Y_2O_3 matrix and ZnPc photosensitizers presents promising solutions to challenges such as phototoxicity and photodegradation, which limit current technologies.[6]

In this paper, we aim to investigate the photophysics of Y_2O_3:$ZnPc(COOH)_4$ by characterizing and analyzing the photophysical properties of this assembly. $ZnPc(COOH)_4$ was chosen for its ability to adsorb onto the surface of Y_2O_3 NPs, enabling the development of a new class of versatile multifunctional nanoparticles for both diagnostic imaging and therapeutic applications.

Experimental

Preparation of Yttrium Oxide Nanoparticles (Y_2O_3)

Yttrium oxide nanoparticles (Y_2O_3) were synthesized using a co-precipitation method assisted by hydrolysis. The precursor material, yttrium nitrate hexahydrate ($Y(NO_3)_3 \cdot 6H_2O$), was dissolved in distilled water to create a 0.1 M aqueous solution. This solution was placed in a flask equipped with a reflux condenser and subjected to hydrolysis at 100°C for 60 hours, ensuring partial hydrolysis of the yttrium nitrate. After hydrolysis, an appropriate amount of ammonium hydroxide (NH_4OH) was added to the hydrolyzed solution, facilitating the precipitation of yttrium hydroxide ($Y(OH)_3$). The amount of ammonium hydroxide added was calculated stoichiometrically to ensure that an excess of 1.5 times the required amount was used, based on the amount of yttrium in the solution. Typically, 0.045 mol of NH_4OH (in 25% concentration) was diluted in a 1:10 ratio with distilled water. The ammonium hydroxide was added in 3–4 portions, with constant stirring over a period of approximately 1 hour, to allow for complete precipitation of $Y(OH)_3$. The precipitate was then washed several times with distilled water (5 times, 20 mL each) to remove any residual impurities. Once the washing was complete, the wet precipitate was dried at room temperature for 2–3 days to remove excess moisture. The obtained $Y(OH)_3$ was then subjected to calcination at 500°C, 600°C, and 700°C for 1 hour in air. The purpose of calcination at different temperatures was to study the impact of temperature on the crystallization, particle size, and phase purity of the Y_2O_3 nanoparticles. The choice of three different calcination temperatures ensures the production of nanoparticles with varying crystalline structures, allowing for a comprehensive evaluation of their properties.

Preparation of ZnPc-(COOH)$_4$

ZnPc-(COOH)$_4$ was synthesized by a melting method followed by basic hydrolysis.[15] To obtain a pure product with high yield, we performed the reaction at high temperature, where all the reactants were melted. Trimellitic anhydride (50 mmol), urea (0.5 mol), ammonium molybdate (0.1 mmol) as a catalyst, and anhydrous zinc salts were placed into a three-necked flask equipped with a reflux condenser. After blending, the reaction temperature increased gradually from 160°C to 230°C over 6 hours and was maintained at 230°C for an additional 2 hours. The mixture was then cooled to room temperature. The resulting mixture was boiled in a 5% hydrochloric acid solution for 1 hour and then filtered. The residue was washed with anhydrous ether and methanol until the filtrate became colorless. After washing to neutrality, tetraamide zinc phthalocyanine was obtained. The compound was dissolved in a NaOH-saturated NaCl solution, refluxed, and stirred for 24 hours at 100°C. The pH of the solution was adjusted to 2 using 5% hydrochloric acid, and the resulting precipitate was separated through static precipitation. The precipitate was washed with ethanol and water to neutrality and then dried in a vacuum oven at 65°C and 0.06 MPa for 3 hours.

Conjugation of Y_2O_3 Nanoparticles with ZnPc-(COOH)$_4$

Zinc-tetracarboxy-phthalocyanine immobilized onto Y_2O_3 NPs was synthesized via a simple immersion method. Y_2O_3 NPs were functionalized by mixing their solution with a ZnPc(COOH)$_4$ solution at an optimal molar ratio. The surface interaction occurred via the coordination bond between the zinc atoms of phthalocyanine and oxygen atoms of Y_2O_3. Due to the fact, that Y_2O_3 NPs have potential applications in medical imaging, drug delivery, and radiation therapy, particularly in the treatment of cancer,

$ZnPc(COOH)_4$ was dissolved in DMSO/H_2O, DMSO/physiological saline, or DMSO/NMP/H_2O mixtures to ensure optimal solubility and to facilitate efficient interaction with Y_2O_3 NPs, where NMP stands for N-methyl-2-pyrrolidone. DMSO was chosen as the primary solvent due to its strong ability to dissolve organic compounds such as $ZnPc(COOH)_4$, ensuring a homogeneous solution. The addition of water or aqueous solutions, such as physiological saline or NMP, provided a good balance between solubility and stability, ensuring efficient dissolution of $ZnPc(COOH)_4$ while maintaining its integrity. The all chosen solutions simulate biological conditions, making it ideal for potential biomedical applications. The Y_2O_3 NPs are dispersed in water, which makes the material safer to handle and more environmentally friendly compared to solvent-based dispersions. Then Y_2O_3 NPs were functionalized by mixing their solution with a solution of $ZnPc(COOH)_4$ at an 1:1 molar ratio. The mixture was stirred at room temperature for one hour, an essential step to ensure efficient interaction between the Y_2O_3 NPs and the ZnPc derivative.

Equipment

The Lambda 25 UV-Vis spectrophotometer (Perkin Elmer Inc., Shelton, CT, USA) was used to record UV-Vis absorption spectra of solutions in the range of 200 nm to 1200 nm using 10 mm quartz cuvettes. The system provides precise absorption data with a 1 nm spectral resolution, optimized for accurate optical property evaluation. Steady-state fluorescence was measured using the LS55 spectrometer (Perkin Elmer Inc.), equipped with double-grating excitation and emission monochromators. The excitation and emission wavelengths were selected with a 5 nm bandwidth for optimal fluorescence intensity and peak accuracy. Fluorescence lifetimes were obtained with Time-

Correlated Single Photon Counting (TCSPC) using the Edinburgh FLS980 spectrometer (Livingston EH54 7DQ, Oxford, UK). The instrument features a < 50 ps temporal resolution, with pulsed diode lasers for excitation, providing detailed analysis of fluorescence decay at room temperature (295 ± 1 K).

The X-ray diffraction (XRD) analysis was performed using an Empyrean diffractometer (PA Nalytical, Netherlands) with CuKα radiation (λ = 1.5406 Å), located at the Regional Interdisciplinary Scientific-Educational Center for the Study of Advanced Materials (CaRISMA) at the Moldova State University (MSU). The system features a Theta-Theta goniometer with a 240 mm radius and a step size of 0.0001° (theta). Data was collected in the 2θ range from 10° to 90° with a 0.02° step size and analyzed using Bruker EVA software. FTIR spectra were recorded using a Bruker ALPHA Platinum-ATR spectrophotometer (Bruker Optik GmbH, Germany), located at the Advanced Materials in Biopharmaceuticals and Engineering at MSU. The spectra were recorded in the 4000 cm^{-1} to 400 cm^{-1} range with a 4 cm^{-1} resolution and an average of 24 scans per measurement to allow for detailed analysis of the functional groups and chemical bonds present in the samples. This Fourier Transform Infrared (FTIR) spectrometer provides precise identification and characterization of chemical compositions, using the ATR (Attenuated Total Reflectance) technique for direct surface analysis of materials.

Results and Discussion

Study of Yttrium Oxide Nanoparticles (Y_2O_3)

XRD analysis of Y_2O_3 NPs presented in Fig. 1.a, revealed a clear correlation between the calcination temperature and the crystalline properties of the material. XRD patterns confirmed the formation of a

single-phase cubic Y_2O_3 structure for all samples, with no impurities or secondary phases detected. The cubic phase was identified by the characteristic diffraction peaks (222), (400), and (440), located at diffraction angles of 29.2°, 33.7°, and 48.4°, respectively, in accordance with JCPDS standard #01-083-0927. At a calcination temperature of 500 °C, the diffraction peaks exhibited relatively low intensity, indicating reduced crystallinity. At 600 °C, the precursor was completely converted into cubic Y_2O_3, with no additional phases observed. As the calcination temperature increased to 700 °C, the peaks became more intense and sharper, accompanied by a narrowing of the full width at half maximum (FWHM). This indicated enhanced crystallinity and a significant increase in crystallite size, which grew from 8.7 nm to 17.3 nm and finally to 22 nm, leading to reduced material porosity [15]. The crystallite size was calculated using the Scherrer equation:

$$D = \frac{k\lambda}{\beta cos\vartheta} \quad (1)$$

where: D is the crystallite size, K is the Scherrer constant (typically 0.9), λ is the wavelength of the X-ray radiation (CuK_α = 1.5406 Å), β is the full width at half maximum (FWHM) of the diffraction peak, θ is the Bragg angle.

Table 1. Microstructural parameters: interplanar distance (d) and crystallite size (D) of Y_2O_3 obtained at different calcination temperatures (T).

T, °C	d, Å	FWHM, º	D, nm
500	3.043	0.96	8.7
600	3.039	0.62	17.3
700	3.042	0.40	22.0

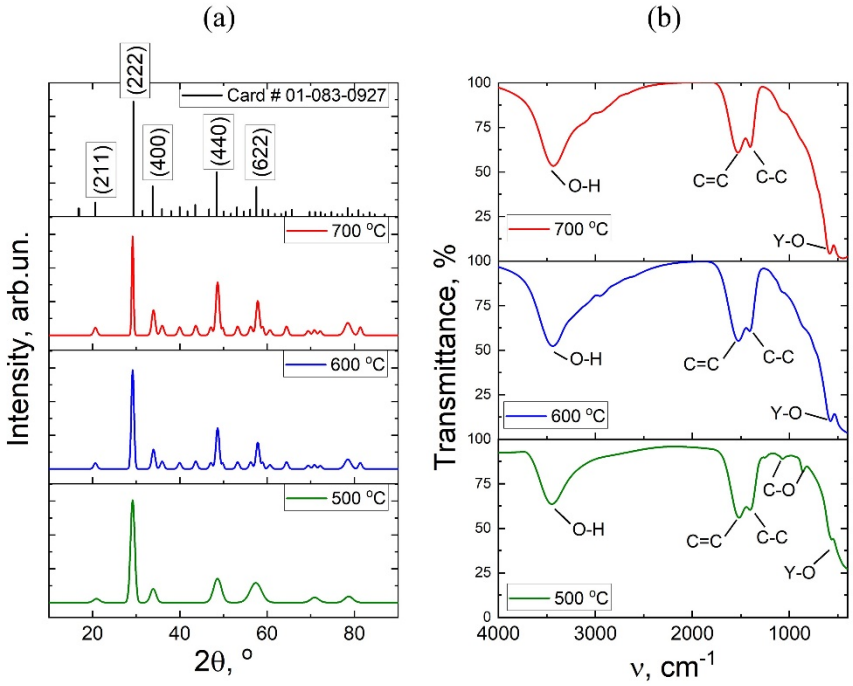

Figure 1. XRD patterns (a) and FTIR analysis (b) of the Y_2O_3 powders calcined at different temperatures.

Figure 1.b presents the infrared (IR) spectra of yttrium precursors calcined at 500 °C, 600 °C, and 700 °C, highlighting the evolution of absorption features with increasing calcination temperature. As the temperature increases, the intensity of absorption peaks related to organic species diminishes, while those associated with metal-oxygen bonds become more pronounced. This shift suggests the progressive decomposition of organic groups and enhanced formation of metal-oxygen bonds during thermal treatment. A notable peak at approximately 3415 cm^{-1} corresponds to O–H stretching vibrations from water molecules.[16] The broadness of this peak is attributed to hydrogen bonding, indicating significant hydration of the precursor. As the calcination temperature surpasses 600 °C, this peak weakens considerably, reflecting the material's gradual dehydration. Additional absorption features include: peaks at

1385 cm^{-1} and 1552 cm^{-1}, which are associated with the stretching vibrations of the organic functional groups C=C and C–C; a peak at 1725 cm^{-1}, corresponding to the stretching vibrations of carbonyl groups.[17]

The peaks at 565 cm^{-1} and 540 cm^{-1} are attributed to Y–O and Y–O–Y bonds, respectively.[18, 19] The Y–O band at 565 cm^{-1} indicates the formation of the yttria phase around 600 °C. An increase in calcination temperature influences the lattice parameter, altering the stretching vibrations of Y–O bonds and shifting their positions in the spectra. These findings confirm that the calcination process facilitates the crystalline development of Y_2O_3 while significantly altering its chemical structure and optical properties, essential for its application in photonics and photodynamic therapy.

The dependence of $(\alpha h\nu)^2 = f(h\nu)$ for Y_2O_3 samples calcined at 500 °C, 600 °C, and 700 °C to determine the band gap energy (E_g) of the material (Figure 2). The results show a slight decrease in the E_g value from 5.54 eV to 5.52 eV as the calcination temperature increases.[20] This trend is consistent with previous observations suggesting that the structural and crystallinity changes induced by the calcination temperature can affect the optical properties of the nanoparticles.

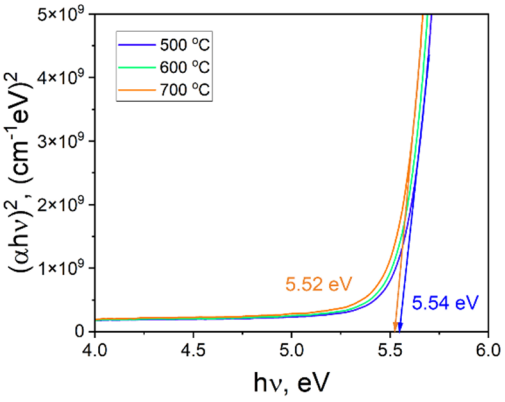

Figure 2. The dependence of $(\alpha h\nu)^2 = f(h\nu)$ for Y_2O_3 samples calcined at 500 °C, 600 °C, and 700 °C.

Photophysics of Y_2O_3 NPs and Y_2O_3:ZnPc(COOH)$_4$ assemblies

The absorption spectra of Y_2O_3:ZnPc(COOH)$_4$ solutions in various solvents such as DMSO/H_2O, DMSO/physiological saline solution, and DMSO/NMP/H_2O are presented in Figure 3, alongside the spectrum of ZnPc(COOH)$_4$. The absorption maxima of ZnPc(COOH)$_4$ lie in the UV and near-infrared regions. The absorption spectra of the ZnPc(COOH)$_4$:Y_2O_3 compound exhibit two bands, the "B" (Soret) band, located around 340 nm, and the "Q" band, positioned between 600 nm and 750 nm. The Q band is split into two sub-bands at 643 nm and 698 nm. This splitting results from the overlapping of electronic transitions associated with the first two excited states and their corresponding vibration levels. Conjugation ZnPc(COOH)$_4$ with Y_2O_3 NPs leads to a decrease in the intensity of the absorption bands in both the UV and NIR (near-infrared) regions.

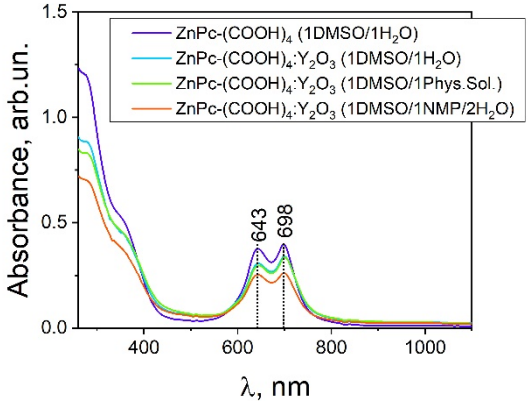

Figure 3. Absorbance of the ZnPc(COOH)$_4$:Y_2O_3 compound in different solvents.

After excitation, the intensity of the light emitted by the compound's atoms decreases exponentially over time, following the equation:

$$I = I_0 \cdot e^{-kt} \qquad (2)$$

where I is the intensity of the fluorescence radiation emitted by the substance, I_0 is the intensity of the incident radiation, k is a characteristic constant of the substance (analogous to a rate constant), and t is the lifetime. The Y_2O_3:ZnPc(COOH)$_4$ solutions emit light as a result of the de-excitation transitions from higher to lower electronic levels following the absorption of electromagnetic radiation at $\lambda = 645$ nm. Substituting ZnPc with the COOH functional group alters the emission wavelength compared to pure ZnPc. The fluorescence emission characteristics recorded in DMSO/H_2O, DMSO/physiological saline, and 2DMSO/NMP/H_2O at a concentration of 1 mg/ml and the excitation wavelengths of 645 nm and 700 nm are illustrated in Figure 4. These spectra show emission bands at 695 nm and between 765 – 771 nm. The fluorescence spectrum is located at longer wavelengths than the absorption spectrum, due to energy losses via vibration relaxation in the excited state. The difference between the absorption band maximum and the fluorescence maximum, known as the Stokes shift, exceeds 50 – 70 nm. The emission spectrum does not depend on the excitation wavelength; illuminating with longer or shorter wavelengths affects only the intensity of the emitted light, without altering its emission profile. A red shift of the fluorescence maximum indicates that the chemical compound is incorporated into hydrophobic environments. When ZnPc(COOH)$_4$ binds to Y_2O_3 nanoparticles in DMSO/H_2O, a variations in the fluorescence emission intensity provide insights into the binding affinity of ZnPc(COOH)$_4$ to Y_2O_3.

Also, the fluorescence intensity of Y_2O_3:ZnPc(COOH)$_4$ in DMSO/physiological saline and 1DMSO/1NMP/H_2O increases considerably. This increase is attributed to intramolecular proton transfer between the carboxy groups and the oxygen atoms in the Y_2O_3 powder, as

well as to the solvent environment, in which the compound is dispersed. The fluorescence emission intensity, and consequently the obtained quantum yields, are significantly higher in spectra recorded in DMSO compared to those in DMSO/H_2O.

The average time molecule remains in the excited state, before emitting a photon, represents its fluorescence lifetime. This parameter was estimated by fitting the decay data using an interactive deconvolution procedure based on the Marquardt algorithm, implemented via software provided by Edinburgh Instruments. The quality of the fit was evaluated using the reduced chi-square (χ^2) test and deviation function criteria. In the organic phase, $ZnPc(COOH)_4$ in DMSO/H_2O displays a bi-exponential decay, clearly indicating the presence of two distinct species populations. In contrast, when $ZnPc(COOH)_4$ is bound to Y_2O_3, the decay becomes mono-exponential, signifying the presence of a single species population.

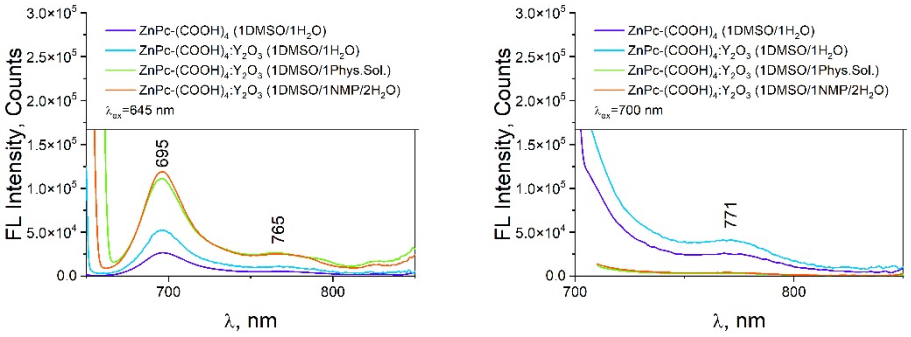

Figure 4. Fluorescence of the Y_2O_3:$ZnPc(COOH)_4$ compound in different solvents.

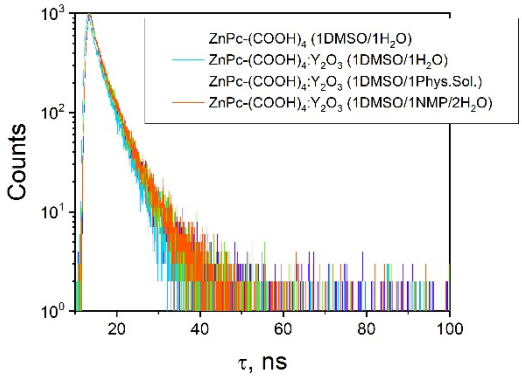

Figure 5. Fluorescence lifetime of the Y_2O_3:ZnPc(COOH)$_4$ compound in different solvents.

Table 2. Fluorescence lifetimes (**τ**) of Y_2O_3:ZnPc(COOH)$_4$ and the quantum yield of fluorescence (**Φ_F**) in different solvents (DMSO/phys. saline and DMSO/NMP/H_2O).

Samples	**FL**		
	τ_1, ns	**τ_2, ns**	**Φ_F, %**
ZnPc-(COOH)$_4$ (*1DMSO/1H_2O*)	1.40	4.08	0.30
ZnPc-(COOH)$_4$:Y_2O_3 (*1DMSO/1H_2O*)	3.07	-	33.44
ZnPc-(COOH)$_4$:Y_2O_3 (*1DMSO/1Phys.Sol*)	3.23	-	10.07
ZnPc-(COOH)$_4$:Y_2O_3 (*1DMSO/1NMP/2H_2O*)	3.05	-	2.09

The fluorescence lifetime of the Y_2O_3:ZnPc(COOH)$_4$ assembly in DMSO/physiological saline and DMSO/NMP/H_2O, as shown in Figure 5, and the corresponding values in Table 2, indicate a mono-exponential decay, with lifetimes twice as long as those of ZnPc(COOH)$_4$ alone. The absolute quantum yield of fluorescence, defined as the ratio between the number of emitted photons and the number of absorbed photons, reaches 0.3% for ZnPc(COOH)$_4$ in DMSO/H_2O, while its binding to Y_2O_3 in the

same solvent increases the yield to 33.44%. Because the spin-orbit coupling of the Y_2O_3:ZnPc(COOH)$_4$ compound is non-zero, it also exhibits phosphorescence. Phosphorescence, or persistent luminescence, has attracted special attention in molecular imaging and detection, since this emission can last for a period after the excitation source is removed, allowing real-time in vivo imaging without external excitation.

Compared to fluorescence-based methods, room-temperature phosphorescence offers several significant advantages for optical detection, including enhanced selectivity and sensitivity, longer emission lifetimes, and a greater spectral shift between excitation and emission spectra. The extended lifetime of the triplet excited state facilitates the development of relatively inexpensive detection systems based on decay time measurements. Moreover, measuring the delayed emission after excitation makes it possible to eliminate spectral interference originating from the system and from light scattering. The combination of nanoparticles with exceptional optical characteristics and the benefits provided by phosphorescence justifies the growing interest in synthesizing and applying new phosphorescent NPs. These are employed in the development of optical sensors and luminescence-based imaging systems. Figure 6 shows the phosphorescence spectra in different solvents, as well as their deconvolution.

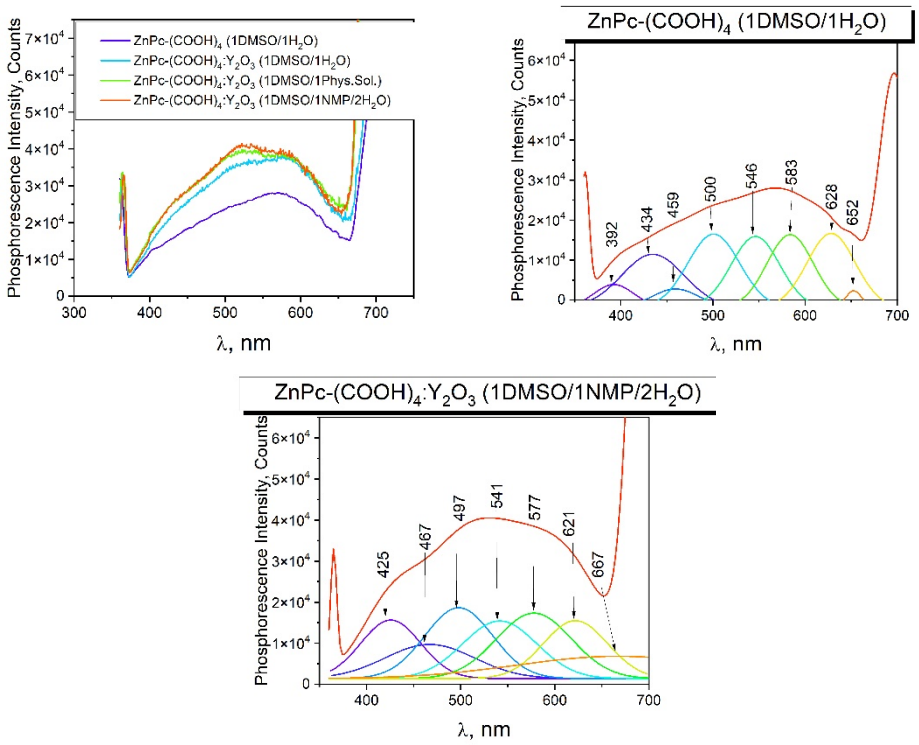

Figure 6. Phosphorescence of the Y_2O_3:ZnPc(COOH)$_4$ compound in different solvents.

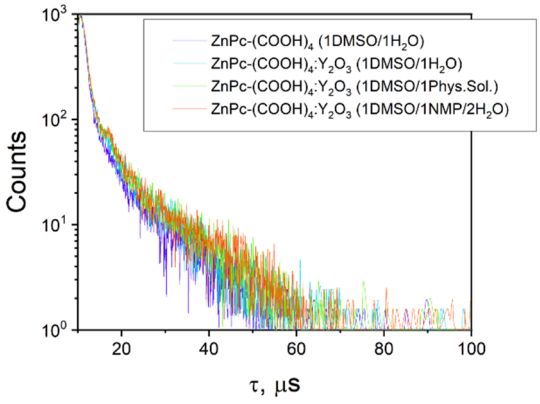

Figure 7. Triplet excited state lifetimes of the Y_2O_3:ZnPc(COOH)$_4$ compound in different solvents.

Table 3. Phosphorescence lifetimes (**τ) and** the triplet quantum yield (**Φ_T)** of $ZnPc(COOH)_4$ and Y_2O_3:$ZnPc(COOH)_4$ in various solvents.

Samples	Phosphorescence		
	τ_1, μs	τ_2, μs	Φ_T, %
$ZnPc\text{-}(COOH)_4$ (*1DMSO/1H_2O*)	1.18	8.89	14.80
$ZnPc\text{-}(COOH)_4$:Y_2O_3 (*1DMSO/1H_2O*)	1.14	9.10	7.29
$ZnPc\text{-}(COOH)_4$:Y_2O_3 (*1DMSO/1Phys.Sol*)	1.18	9.78	29.87
$ZnPc\text{-}(COOH)_4$:Y_2O_3 (*1DMSO/1NMP/2H_2O*)	1.30	10.37	30.88

The triplet excited state lifetime of the Y_2O_3:$ZnPc(COOH)_4$ compound, under 355 nm excitation, displays a bi-exponential decay. The corresponding lifetime values are presented in Table 3. For the $ZnPc(COOH)_4$:Y_2O_3 assembly in a 1DMSO/1NMP/2H_2O solvent, the highest lifetime values, 1.3 μs and 10.4 μs, are recorded. The phosphorescence quantum yield of this compound reaches 30.88%.

To sum up, room-temperature phosphorescent $ZnPc(COOH)_4$:Y_2O_3 assembly is useful in optical imaging and sensing technologies.

Potential Application of $ZnPc(COOH)_4$:Y_2O_3 assemblies

The findings from the study on the Y_2O_3:$ZnPc(COOH)_4$ assembly reveal significant potential across various applications, particularly in photodynamic imaging, optical sensors, optoelectronic devices, and biomedical therapies. The unique properties of this assembly, characterized by enhanced fluorescence and phosphorescence, position it favorably against similar systems, such as those utilizing ZnPc alone or other conventional systems. The functionalization of Y_2O_3 NPs with $ZnPc(COOH)_4$ not only improves the photophysical characteristics but also

enhances the biological compatibility of the system, making it a frontrunner for advanced optical and biomedical technologies.

Also, the Y_2O_3:ZnPc(COOH)$_4$ assembly demonstrates significantly enhanced fluorescence lifetimes, which can improve the sensitivity and resolution of fluorescence imaging. Compared to systems like ZnPc alone, the incorporation of Y_2O_3 NPs facilitates better energy transfer between both, leading to increased fluorescence yield. This enhancement is crucial for in vivo imaging applications, where high sensitivity and low background noise are paramount for accurate diagnostics.[21] The integration of Y_2O_3 nanoparticles not only enhances the imaging capabilities but also contributes to the therapeutic efficacy of PDI, making it a versatile tool in oncological diagnostics and treatment.[22]

The optical sensing capabilities of the Y_2O_3:ZnPc(COOH)$_4$ assembly are promising due to its excellent fluorescence and phosphorescence characteristics. The increased fluorescence lifetime and stability in various solvents make it suitable for detecting gases, environmental pollutants, or biomarkers. The incorporation of Y_2O_3 nanoparticles improves the dispersion of ZnPc(COOH)$_4$, enhancing the signal-to-noise ratio in optical sensing devices. This is particularly advantageous compared to systems lacking such nanostructuring, which often suffer from poor light absorption and energy transfer efficiency.[23, 24]

The high stability and enhanced photoluminescence properties suggest its applicability in light-harvesting applications, particularly when compared to conventional organic semiconductors.[25] For example, the integration of Y_2O_3 with ZnPc(COOH)$_4$ in organic light-emitting diodes (OLEDs) can lead to improved efficiency and longer device lifetimes, as the

assembly's tunable fluorescence properties allow for greater flexibility in device design.[26]

The combination of Y_2O_3 NPs with $ZnPc(COOH)_4$ holds substantial promise in biomedical therapies, particularly in photodynamic therapy (PDT) for cancer treatment. The enhanced fluorescence properties and increased fluorescence lifetimes of this assembly allow for improved tissue penetration and targeted therapy. Compared to systems that utilize only ZnPc or other organic photosensitizers, the incorporation of Y_2O_3 NPs provides a more stable and efficient energy transfer system, that contribute to the increasing of generation of ROS under light excitation.[27, 28]

Conclusions

This study revealed that binding $ZnPc(COOH)_4$ to Y_2O_3 NPs leads to a significant increase in fluorescence intensity, suggesting the formation of stable chemical bonds between the two components. The optical properties of the Y_2O_3:$ZnPc(COOH)_4$ hybrid systems-exhibiting enhanced fluorescence and phosphorescence, triplet excited state lifetimes of up to 1.3 μs and 10.4 μs, as well as high quantum yields (up to 33.44% for fluorescence and 30.88% for phosphorescence) - demonstrate their potential for applications in photodynamic imaging, optical sensors, optoelectronic devices, and biomedical therapies.

Furthermore, it was found that the solvent environment and synthesis parameters significantly influence the spectral and photophysical characteristics, offering opportunities to optimize and tailor these materials for specific requirements. Consequently, these findings open new perspectives for further research and the development of other types of

nanoparticles, photosensitizers, and dopants aimed at obtaining advanced materials for industrial and medical applications.

Acknowledgements

This paper was financially supported by the National Agency for Research and Development of the Republic of Moldova, project "Nanoparticles Doped with Rare Earth Elements for Applications in Biomedical Imaging and Cancer Cell Therapy" #20.80012.5007.22SE.

References

1. Qi, L.; Gao, X. Emerging application of quantum dots for drug delivery and therapy. *Expert Opin. Drug Deliv.* **2008**, *5*(3), 263 – 267. https://doi.org/10.1517/17425247.5.3.263
2. Medintz, I. L.; Mattoussi, H.; Clapp, A. R. Potential clinical applications of quantum dots. *Int. J. Nanomed.* ***2008***, *3*(2), 151 – 167. https://doi.org/10.2147/ijn.s614
3. Smith, A. M.; Ruan, G.; Rhyner, M. N.; Nie, S. Engineering luminescent quantum dots for in vivo molecular and cellular imaging. *Ann. Biomed. Eng.* **2006**, *34*, 3 – 14. https://doi.org/10.1007/s10439-005-9000-9
4. Chan, W. C.; Maxwell, D. J.; Gao, X.; Bailey, R. E.; Han, M.; Nie, S. Luminescent quantum dots for multiplexed biological detection and imaging. *Curr. Opin. Biotechnol.* **2002**, *13*(1), 40 – 46. https://doi.org/10.1016/S0958-1669(02)00282-3
5. Hirata, G. A.; McKittrick, J.; Avalos-Borja, M.; Siqueiros, J. M.; Devlin, D. Physical properties of Y_2O_3:Eu luminescent films grown by MOCVD and laser ablation. *Appl. Surf. Sci.* **1997**, *113*, 509 – 514. https://doi.org/10.1016/S0169-4332(96)00829-X
6. Dhanaraj, J.; Jagannathan, R.; Kutty, T. R. N.; Lu, C. H. Photoluminescence characteristics of Y_2O_3:Eu^{3+} nanophosphors prepared using sol–gel thermolysis. *J. Phys. Chem. B*. **2001**, *105*(45), 11098 – 11105. https://doi.org/10.1021/jp0119330
7. Li, X. -P.; Qi, Y.; Zhang, J. -S.; et al. Synthesis and size-dependent luminescence properties of Y_2O_3:Eu^{3+} nanospheres. *Chin. J. Lumin.* **2017**, *38*, 139 – 146. https://doi.org/10.3788/fgxb20173802.0139

8. Sekkat, N.; van den Bergh, H.; Nyokong, T.; Lange, N. Like a bolt from the blue: Phthalocyanines in biomedical optics. *Molecules* **2011**, *17*(1), 98 – 144. https://doi.org/10.3390/molecules17010098

9. Fraçkowiak, D.; Planner, A.; Wiktorowicz, K. Near-infrared applications in medicine. In *Near-Infrared Applications in Biotechnology*; CRC Press, **2020**, pp. 151 – 183. https://doi.org/10.1201/9780429132650-6

10. Minnock, A.; Vernon, D. I.; Schofield, J.; Griffiths, J.; Parish, J. H.; Brown, S. B. Photoinactivation of bacteria: Use of a cationic water-soluble zinc phthalocyanine to photoinactivate both gram-negative and gram-positive bacteria. *J. Photochem. Photobiol. B: Biol.* **1996**, *32*(3), 159 – 164. https://doi.org/10.1016/1011-1344(95)07148-2

11. Lukyanets, E. A. Phthalocyanines as photosensitizers in the photodynamic therapy of cancer. *J. Porphyrins Phthalocyanines* **2012**. https://doi.org/10.1002/(SICI)1099-1409(199908/10)3:6/7%3C424::AID-JPP151%3E3.0.CO;2-K

12. Bonnett, R. *Chemical Aspects of Photodynamic Therapy*; CRC Press: **2000**. https://doi.org/10.1201/9781482296952

13. Triesscheijn, M.; Baas, P.; Schellens, J. H.; Stewart, F. A. Photodynamic therapy in oncology. *Oncologist* **2006**, *11*(9), 1034 – 1044. https://doi.org/10.1634/theoncologist.11-9-1034

14. Back, M.; Massari, A.; Boffelli, M.; Gonella, F.; Riello, P.; Cristofori, D.; … Enrichi, F. Optical Investigation of Tb^{3+}-Doped Y_2O_3 Nanocrystals Prepared by Pechini-Type Sol–Gel Process. *J. Nanopart. Res*. **2012**, *14*(4). https://doi.org/10.1007/s11051-012-0792-x

15. Potlog, T.; Popusoi, A.; Lungu, I.; Robu, S.; Bulimestru, I. Photophysics of Tetracarboxy-Zinc Phthalocyanine Photosensitizers. *RSC Adv*. **2022**, *12*(49), 31778 – 31785. https://doi.org/10.1039/D2RA05676C

16. Chen, S.; Lin, J.; Wu, J. Facile Synthesis of Y_2O_3:Dy^{3+} Nanorods and Its Application in Dye-Sensitized Solar Cells. *Appl. Surf. Sci*. **2014**, *293*, 202 – 206. https://doi.org/10.1016/j.apsusc.2013.12.134

17. Wang, S.; An, C.; Zhang, Y.; Zhang, Z.; Qian, Y. Ethanothermal Reduction to MoO_2 Microspheres via Modified Pechini Method. *J. Cryst. Growth* **2006**, *293* (1), 209 – 215. https://doi.org/10.1016/j.jcrysgro.2006.05.007

18. Aghazadeh, M.; Ghaemi, M.; Nozad Golikand, A.; Yousefi, T.; Jangju, E. Yttrium Oxide Nanoparticles Prepared by Heat Treatment of Cathodically Grown Yttrium Hydroxide. *Int. Scholarly Res. Notices* **2011**, *2011*, 542104. https://doi.org/10.5402/2011/542104

19. Wang, N.; He, J. Color-Tunable Infrared-to-Visible Upconversion Luminescence and Intensified 1.54 μm Near-Infrared Emission in Y_2O_3: Yb^{3+}, Er^{3+}, Eu^{3+} Phosphors Prepared by Sol-Gel Method. *J. Lumin.* **2023**, *257*, 119718. https://doi.org/10.1016/j.jlumin.2023.119718

20. Ahmad, S.; Faizan, M.; Ahmad, S.; Ikram, M. Synthesis and Characterization of Y_2O_3 Nano-Material: An Experimental and Theoretical Study. *DAE Solid State Phys. Symp.* **2018**.

21. Wang, W.; Wang, J.; Hong, G.; Mao, L.; Zhu, N.; Liu, T. Methoxypolyethylene glycol-substituted zinc phthalocyanines for multiple tumor-selective fluorescence imaging and photodynamic therapy. *Biomacromolecules*. **2021**, *22*(10), 4284 – 4294. https://doi.org/10.1021/acs.biomac.1c00855

22. Meng, J.; Cui, Y.; Wang, Y. Rare Earth-Doped Nanoparticles for Near-Infrared II Image-Guided Photodynamic Therapy. *ACS Appl. Nano Mater.* **2024**, *7*(9), 11008 – 11018. https://doi.org/10.1021/acsanm.4c021763010

23. Zhou, L.; Chen, E.; Jin, W.; Wang, Y.; Zhou, J.; Wei, S. Monomer zinc phthalocyanine/upconversion nanoparticle coated with hyaluronic acid crosslinked gel as NIR light-activated drug for in vitro photodynamic therapy. *Dalton Trans.* **2016**, *45*(38), 15170 – 15179. https://doi.org/10.1039/C6DT01929C

24. Ong, W. K.; Yao, X.; Jana, D.; Li, M.; Zhao, Y.; Luo, Z. Efficient production of reactive oxygen species from Fe3O4/ZnPC coloaded nanoreactor for cancer therapeutics in vivo. *Small Struct.* **2020**, *1*(3), 2000065. https://doi.org/10.1002/sstr.202000065

25. Arena, D.; Nguyen, C.; Ali, L. M.; Verde-Sesto, E.; Iturrospe, A.; Arbe, A.; Pomposo, J. A. Amphiphilic Single-Chain Polymer Nanoparticles as Imaging and Far-Red Photokilling Agents for Photodynamic Therapy in Zebrafish Embryo Xenografts. *Adv. Healthcare Mater.* **2024**, *13*(28), 2401683. https://doi.org/10.1002/adhm.20240168

26. Alam, K. M.; Kumar, P.; Gusarov, S.; Kobryn, A. E.; Kalra, A. P.; Zeng, S.; Shankar, K. Synthesis and characterization of zinc phthalocyanine-cellulose nanocrystal (CNC) conjugates: toward highly functional CNCs. *ACS Appl. Mater. Interfaces*. **2020**, *12*(39), 43992 – 44006. https://doi.org/10.1021/acsami.0c07179223110

27. Liu, J.; Kang, D. W.; Fan, Y.; Nash, G. T.; Jiang, X.; Weichselbaum, R. R.; Lin, W. Nanoscale covalent organic framework with staggered stacking of

phthalocyanines for mitochondria-targeted photodynamic therapy. *J. Am. Chem. Soc.* **2023**, *146*(1), 849 – 857. https://doi.org/10.1021/jacs.3c11092

28. Wang, W.; Wang, J.; Hong, G.; Mao, L.; Zhu, N.; Liu, T. (2021). Methoxypolyethylene glycol-substituted zinc phthalocyanines for multiple tumor-selective fluorescence imaging and photodynamic therapy. *Biomacromolecules*. **2021**, *22*(10), 4284 – 4294. https://doi.org/10.1021/acs.biomac.1c008556050